ARL-TR-9086 ● SEP 2020

DEVCOM ARMY RESEARCH LABORATORY

Synthesis of a Functionalized, Multiarm Spiropyran Mechanophore and Evaluation under Quasi-static and High-Rate Loading Conditions in Bulk PDMS

by James Berry, Yangju Lin, Logan Shannahan, Müge Fermen-Coker, Stephen Craig

NOTICES

Disclaimers

The findings in this report are not to be construed as an official Department of the Army position unless so designated by other authorized documents.

Citation of manufacturer's or trade names does not constitute an official endorsement or approval of the use thereof.

Destroy this report when it is no longer needed. Do not return it to the originator.

ARL-TR-9086 ● SEP 2020

Synthesis of a Functionalized, Multiarm Spiropyran Mechanophore and Evaluation under Quasi-static and High-Rate Loading Conditions in Bulk PDMS

James Berry, Logan Shannahan, and Müge Fermen-Coker,
Weapons and Materials Research Directorate, CCDC Army Research Laboratory

Yangju Lin* and Stephen Craig
Duke University

**** At Stanford University at date of publication***

REPORT DOCUMENTATION PAGE		Form Approved OMB No. 0704-0188

1. REPORT DATE *(DD-MM-YYYY)*	2. REPORT TYPE	3. DATES COVERED (From - To)
September 2020	Technical Report	April 2019–August 2020

4. TITLE AND SUBTITLE

Synthesis of a Functionalized, Multiarm Spiropyran Mechanophore and Evaluation under Quasi-static and High-Rate Loading Conditions in Bulk PDMS

5a. CONTRACT NUMBER

5b. GRANT NUMBER

5c. PROGRAM ELEMENT NUMBER

6. AUTHOR(S)

James Berry, Yangju Lin, Logan Shannahan, Müge Fermen-Coker, Stephen Craig

5d. PROJECT NUMBER

5e. TASK NUMBER

5f. WORK UNIT NUMBER

7. PERFORMING ORGANIZATION NAME(S) AND ADDRESS(ES)

CCDC Army Research Laboratory
ATTN: FCDD-RLW-PC
Aberdeen Proving Ground, MD 21005

8. PERFORMING ORGANIZATION REPORT NUMBER

ARL-TR-9086

9. SPONSORING/MONITORING AGENCY NAME(S) AND ADDRESS(ES)

10. SPONSOR/MONITOR'S ACRONYM(S)

11. SPONSOR/MONITOR'S REPORT NUMBER(S)

12. DISTRIBUTION/AVAILABILITY STATEMENT

Approved for public release; distribution is unlimited.

13. SUPPLEMENTARY NOTES

This report has been edited per the style guide *Scientific Style and Format: The CSE Manual for Authors, Editors, and Publishers*. 8th ed. Chicago (IL): University of Chicago Press; 2014.

14. ABSTRACT

Mechanophores have shown great utility in transforming normally destructive chemistry (bond scission) into productive outcomes. While many examples of mechanophores with two linkages to the polymeric backbone have been divulged in the literature, far less has been studied on mechanophores with four or more bonds to the backbone. In addition, no studies have been reported on the high-rate behavior characterization of these multiarm molecules. Here, we report the synthesis of a functionalized, four-arm spiropyran mechanophore and its incorporation into a bulk elastomeric material: polydimethylsiloxane (PDMS). Quasi-static tensile testing, as well as the first Kolsky bar (high-rate loading) experiments on these specimens, is discussed and compared with two-arm mechanophore substrates, as well as prior work conducted on mechanophore-embedded star polymers.

15. SUBJECT TERMS

mechanophore, spiropyran, polydimethylsiloxane, Kolsky bar, organic synthesis, high-rate material characterization, quasi-static testing

16. SECURITY CLASSIFICATION OF:			17. LIMITATION OF ABSTRACT	18. NUMBER OF PAGES	19a. NAME OF RESPONSIBLE PERSON
a. REPORT	b. ABSTRACT	c. THIS PAGE			James Berry
Unclassified	Unclassified	Unclassified	UU	36	19b. TELEPHONE NUMBER (Include area code) (410) 278-1519

Contents

List of Figures

List of Tables

Acknowledgments

The authors acknowledge the support of the US Army Combat Capabilities Development Command (CCDC) Army Research Laboratory's (ARL's) Weapons and Materials Research Directorate for this work. James Berry thanks Dr Robert Lambeth for helpful technical discussions. James Berry and Yangju Lin contributed equally to this work.

1. Introduction

Mechanophores, small molecules that contain a labile bond, have come to the fore as force-sensitive species that can indicate when a material has experienced an applied load.[1,2] Molecules such as spiropyrans (SPs),[3,4] naphthopyrans,[5] *gem*-dibromocyclopropanes (*g*-DBCs),[6] and coumarin dimers[7] have been used to effect these transformations. While early investigations into this novel area of chemistry were primarily conducted in solution,[8] using sonication to induce cavitation bubbles, there is increasing usage of these mechanophores in bulk systems as force-detection probes.[9] Testing of mechanophores embedded into materials such as poly(methacrylate) (PMA),[10,11] poly(methyl methacrylate) (PMMA),[12,13] polydimethylsiloxane (PDMS),[14–16] polyurethane (PU)[17] and polycarbonate (PC)[18] has been completed, demonstrating the utility of mechanophores as force-sensing entities.

While much emphasis has been placed on mechanophores that have two connections to the polymer backbone to facilitate force transfer across the labile bond, studies involving additional linkages to the backbone have not been as common. The Otsuka group has divulged studies of their work on diarylbibenzofuranone (DABBF), which was incorporated into a star polymer motif using polystyrene (PS) as the bulk material.[19] Here, the DABBF molecule, when exposed to grinding, was found to undergo homolytic cleavage to produce blue arylbenzofuranone (ABF) radicals, which were quite stable in the absence of solvent. Upon exposure to organic solvent, radical recombination occurred to reform the broken bond. It was shown that the greater the number of polymer "arms" (four or eight) connected to the mechanophore, the easier the cleavage of DABBF and subsequent production of the blue radical ABF species. Building on this work, they disclosed the synthesis and evaluation of higher orders of dendrimer species, which were easier to activate due to rigidity of the higher-generation dendrimers. This rigidity is caused by the high surface area (sterics) of the dendrimer, which effectively prevents force attenuation and thus greater force transfer to the mechanochromic DABBF molecule at the core.[20]

The aforementioned branched DABBF studies examine the behavior of these molecules within a rigid polymer, polystyrene powder, through the use of grinding to induce activation. Conversely, the behavior of branched molecules within soft elastomeric materials, such as PDMS, has not yet been addressed. In addition, to the best of our knowledge, no study has been performed in which these branched polymers have been exposed to high rate loading conditions. In this report, we disclose the synthesis of a SP-based mechanophore **1** containing four covalent

linkages to the elastomeric PDMS backbone, and its evaluation under both quasi-static and high-rate loading conditions (Fig. 1).

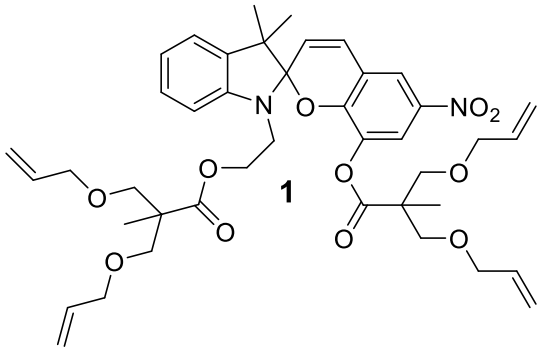

Fig. 1 Four-arm SP 1 used in this study

2. Synthesis of Four-Arm Mechanophore 1

2.1 Attempted Synthesis of 6 Using 4-Pentenoyl Chloride

The synthesis of the base SP (SP-NO_2) **5** has been reported previously.[14–15,21] Since two alkene attachment points are needed on each side of the spirocyclic junction, the use of a readily available commercial material containing two functional handles is necessary. A common starting material, 2,2-bis(hydroxymethyl)propionic acid (bis-MPA) **2,** has been used for the synthesis of dendritic compounds[22] in which successive generations are added in a stepwise manner. Due to its synthetic versatility and ease of use, this molecule was selected for introduction of additional linkages to the SP core (see Appendix for synthetic procedures).

Initial work toward the four-arm SP **6** began with acylation of bis-MPA **2**, using 4-pentenoyl chloride to produce the requisite carboxylic acid **3** (Fig. 2). Conversion of **3** to the acid chloride using oxalyl chloride produced **4**, which was used without purification in the following step. Acylation of SP **5** with crude acid chloride **4** was attempted, but reaction monitoring with thin-layer chromatography (TLC) revealed a mixture of multiple products from which **6** could not easily be isolated.

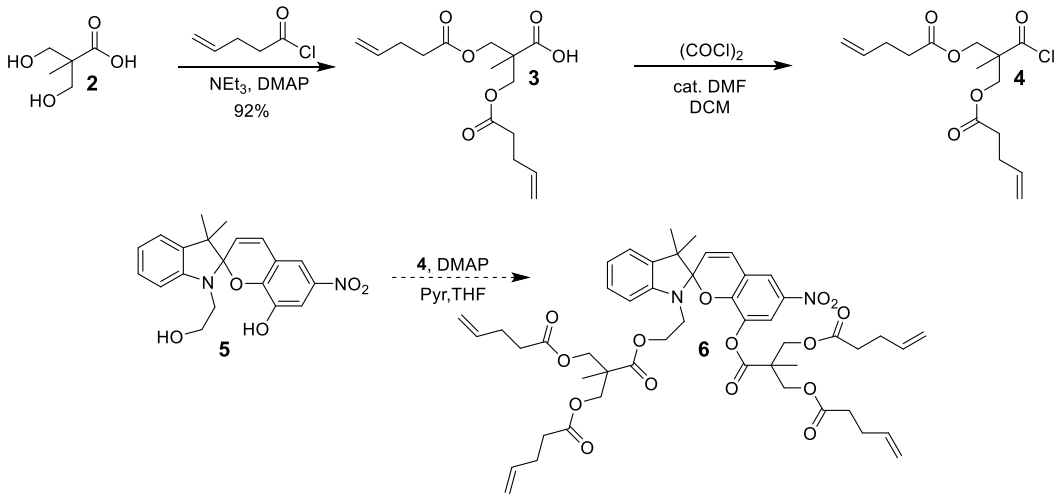

Fig. 2 Attempted synthesis of four-arm SP 6

2.2 Synthesis of 1 Using Allyl Bromide

Since the acid chloride may be too reactive for acylation of **5**, a milder acylating agent, the acid anhydride, was employed. Also, to further prevent unwanted side reactions, in addition to providing a more robust substrate, the pentenoate ester of **3** was replaced with an allyl ether group. The synthesis began with alkylation of bis-MPA **2** with allyl bromide under basic conditions[23] to give **7** (Fig. 3). Acid anhydride formation using dicyclohexylcarbodiimide (DCC)[23] provided **8** in high yield as a light-yellow oil. However, when a solution of **8** in tetrahydrofuran (THF) was added to a solution of **5** and *N*,*N*-dimethylaminopyridine (DMAP) in THF and stirred overnight, chromatography revealed two very close spots on the TLC plate. While both spots were active under UV light development, the lower R_f spot (R_f = 0.76 in 1% methanol [MeOH] in dichloromethane [DCM]) produced the characteristic orange/red color indicative of an SP after exposure to UV light. Unfortunately, column chromatography proved difficult in providing clean samples of the two major products. Based on ^{1}H-NMR (nuclear magnetic resonance) spectroscopy of the mixture, it was hypothesized that the higher spot on the TLC plate could be an overacylated product, in which the resulting phenoxide (from SP ring-opening due to its solvatochromic properties) reacts with an additional molecule of **8**. This would result in an acylated merocyanine structure that is incapable of reforming the spirocyclic C–O bond. Recently, this type of overacylation has been shown to take place in related systems, and the undesired side reaction was attenuated through slow (over 4 h) addition of the acylating agent to the SP.[18] This protocol was employed and one product spot was seen on TLC. After workup and purification, target SP **1** was isolated in 36% yield (Fig. 3).

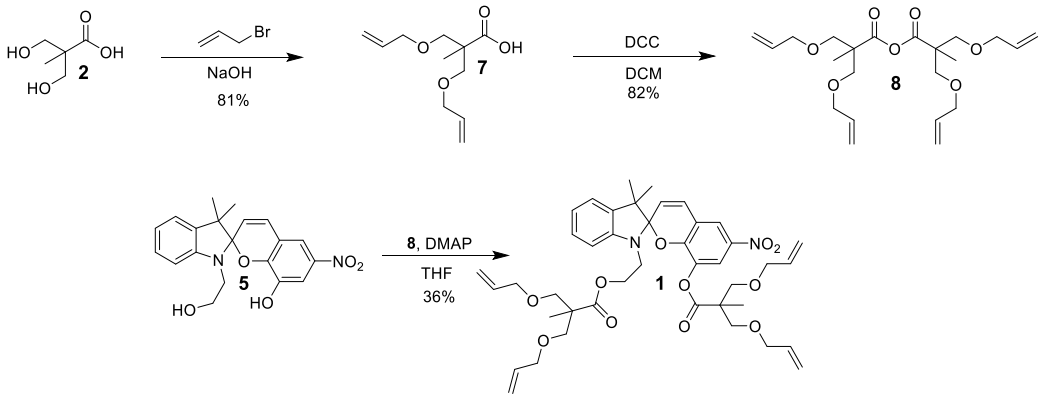

Fig. 3 Synthetic scheme for four-arm SP 1

2.3 Curing of 1 and 9 into PDMS

2.3.1 Quasi-static Experiments

A corresponding amount of **t-SP** (**1**) or **b-SP** (**9**)[15] (Fig. 4) was dissolved in 0.25 mL of xylene, and 2.0 g of Sylgard 184 base was added to the mechanophore solution. The mixture was thoroughly vortexed for 3 min, and then 0.2 g Sylgard 184 curing agent was added. The resulting mixture was further vortexed for 3 min. After degassing under house vacuum, the pale-pink mixture was poured onto a polyester film and cured at 65 °C overnight. A clear PDMS film was obtained after cooling to room temperature. *Note that the molar number of SP mechanophores in* ***t-SP_A*** *is the same as that of* ***b-SP****, whereas the molar number of alkene groups in* ***t-SP_B*** *is the same as that of* ***b-SP*** (Table 1).

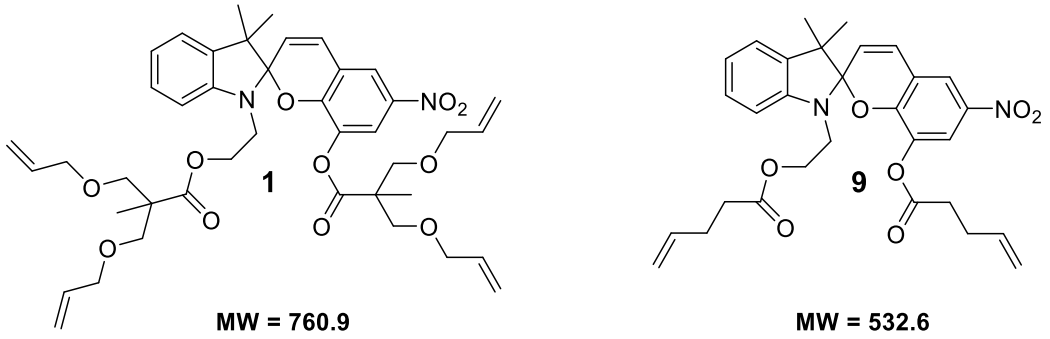

Fig. 4 Four-arm mechanophore t-SP (1) and two-arm mechanophore b-SP (9) used in this study

Table 1 Composition of Sylgard 184 PDMS elastomer embedded with mechanophores 1 or 9

Mechanophore	M	wt%	m (mg)	n/mol	n (alkene)/mol	PDMS (m)
b-SP (9)	532.6	0.5	11	2.06e-5	4.12e-5	2.2 g
t-SP_A (1)	760.9		15.7	2.06e-5	8.24e-5	
t-SP_B (1)			7.8	1.03e-5	4.12e-5	

2.3.2 High-Rate Experiments

To create the samples used in the high-rate testing experiments, the previously disclosed procedure was used.[15] A final SP (**1** or **9**) concentration of 0.5 weight% in PDMS was employed, allowing for creation of five cylindrical samples of 0.25-inch diameter and 1.5 inches in length, from which the requisite Kolsky samples were cut.

3. Quasi-static Testing

3.1 Experimental Considerations

Quasi-static Tensile Tests

PDMS films containing SP **1** or **9** were cut into strips (5 × 1 cm, 300–500 μm thick) and subjected to tensile tests using a TA Instruments RSA III Dynamic Mechanical Analyzer at strain rate of 0.5 mm s^{-1}. The raw color images at various strains were recorded on a Canon EOS Rebel XSi camera.

Analysis

The relative activation of SP was determined through image analysis, as reported previously.[24] In a typical image analysis (Fig. 5), the image of a strained sample was analyzed from the red, green, and blue channel, and the average pixel intensity from the same region of interest was obtained. The strain was calculated from the length of specimen relative to its initial length.

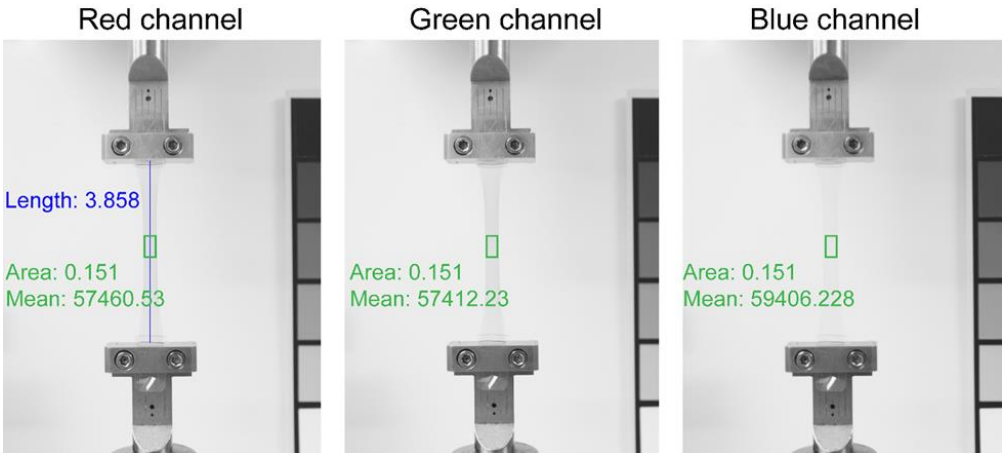

Fig. 5 Representative image analysis of a strained PDMS sample. The average pixel intensity from each channel was obtained and the strain was calculated from the measured length of the stretched sample, as indicated in the red channel.

To rule out variance in the background, the ratios of channel intensities were evaluated and further used to determine the relative activation over strain. As shown in Fig. 6, the value of B/R, which denotes the ratio of pixel intensity obtained from blue and red channels, gave the best signal-to-noise ratio and was applied for further analysis.

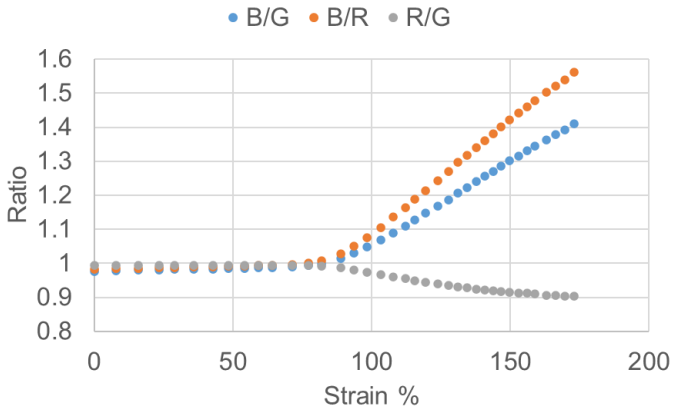

Fig. 6 Ratios of pixel value obtained from each channel were plotted as a function of strain. The B/R value gave the best signal and was used for further analysis.

3.2 Results

As shown in Fig. 7, there is a slight difference in tensile properties as a function of mechanophore. In particular, the average stress–strain behavior of **t-SP_B** shows a slightly higher initial modulus and slightly lower onset for strain hardening than is observed in **t-SP_A**. The **b-SP** elastomer, in comparison, exhibits both a lower initial modulus and a higher strain at the strain-hardening onset than the samples

made with the tetra-alkene mechanophores. Possible reasons for the difference in behavior are discussed in the following sections.

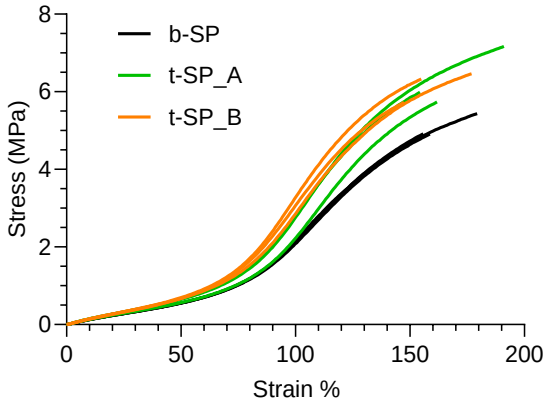

Fig. 7 Stress–strain curves of PDMS elastomers incorporated with SP mechanophores, which are comprised of two (b-SP, compound 9) or four (t-SP, compound 1) alkene linkage arms. The molar number of SP in t-SP_A is the same as b-SP, whereas the molar number of alkenes in t-SP_B is identical to b-SP (Table 1). The figure shows the overlay of three stress–strain curves for each sample.

The increase in B/R, that is, Δ(B/R), was used to indicate the relative activation of SP in the PMDS samples. A representative overlay of Δ(B/R) versus strain for three samples is shown in Fig. 8. The Δ(B/R) values remain nearly unchanged near 0 in the strain range of 0 to approximately 90%. As the strain increases, the Δ(B/R) values increase linearly as a function of strain. The relative activation in the three samples follows the trend of **b-SP** > **t-SP_A** > **t-SP_B** in the strain range of 90 to approximately 175%. Back extrapolation of the relative activation to the "zero" activation point gives the activation onset as approximately 90% strain in all samples, near the strain at which strain hardening sets in. It should be noted that the three samples under investigation possess a similar activation onset. At approximately 175% strain, the Δ(B/R) values for **b-SP**, **t-SP_A**, and **t-SP_B** are 0.58, 0.44, and 0.22, respectively (Fig. 8). Because the electronics of the different cross-linking arms are similar, the extinction coefficient of the mechanophores are expected to be similar. Thus, the relative activation of the mechanophore at 175% uniaxial strain in these three samples is approximately 2.6:2:1.

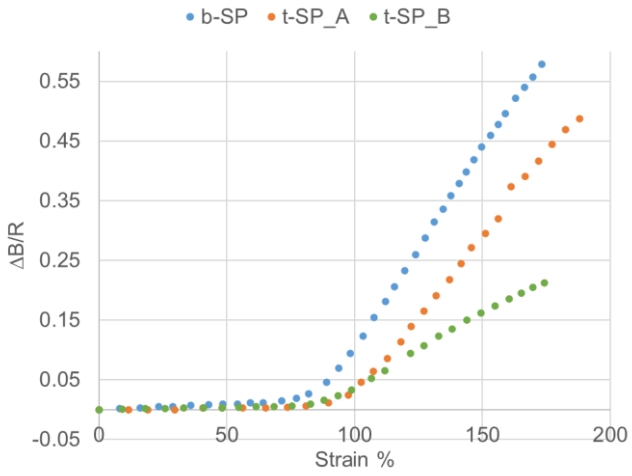

Fig. 8 Typical overlay of Δ(B/R) vs. strain plots for b-SP, t-SP_A, and t-SP_B samples

4. High-Rate Testing

4.1 Experimental Considerations

High-rate characterization of the SP-embedded PDMS samples was carried out using a compression Kolsky bar.[25] Samples were prepared by cutting molded blanks into individual samples with a nominal length of 5 mm and diameter of 9.5 mm. These cuts were made using a custom fixture in which the sample blank was placed into two bearings with diameters slightly larger than the sample and a razor blade inserted into the gap between the two bearings, providing a perpendicular cut while minimizing bending and other deformation of the sample blank. This fixture was used to ensure that the opposite faces of the samples were as parallel as possible, which is a necessity, since polishing to final dimensions and parallelism was not a feasible option for this material.

The Kolsky bar system used a polycarbonate bar instead of more typical steel or aluminum to provide a material better matched in properties to the sample and to also ensure that a sufficiently large strain signal was generated in the bar. Polycarbonate is viscoelastic, and as such, a viscoelastic correction for the recorded strain signals was implemented following Bacon's method.[26] The longitudinal wave speed of the Kolsky bar was experimentally measured and found to be 1821 ms^{-1}. The bar diameter was 12.4 mm. The striker was made of polycarbonate as well, and had a length of 0.5 m and a diameter of 9.5 mm. All tests were conducted at a standard firing pressure of 30 psi. Mineral oil was used as a lubricant between the sample and the bar to reduce frictional effects. Force equilibrium was checked during analysis to confirm that each experiment was valid.

To record color change, high-speed color photography of each test was captured and synced in time with the recorded strain data from the Kolsky bar. A Phantom v2012 camera operating at 100,000 frames per second and a resolution of 512 × 320 pixels was aligned perpendicular to the Kolsky bar and triggered off of the same optical sensor as the data collection. The sample was backlit by a Multiled LT-V9-15 LED lamp, ensuring constant illumination throughout the experiment.

Computer image analysis was used to calculate the onset time of color change based on the high-speed color imagery. In this methodology, representative examples of the background color, bar color, and sample were selected at the beginning of analysis of each sample. For the entire range of captured images, each pixel in each image was then classified as background, bar, or sample, based on a nearest-neighbor method. As the background is white and the bars are black, this resulted in consistent detection of the sample throughout the experiment. For each image, the color value of the selected sample pixels was averaged and recorded. CIELAB color space was used as it provides a separate illumination channel in addition to the red-green and blue-orange channels. The time series of the average color value of the sample in each color channel over the duration of the experiment was then used to determine a characteristic feature matching onset of color change, similar to the method described in the literature.[15] However, in this case, a local minimum prior to a large spike in the measured blue-orange color signal was found to be the best indicator, as shown in Fig. 9.

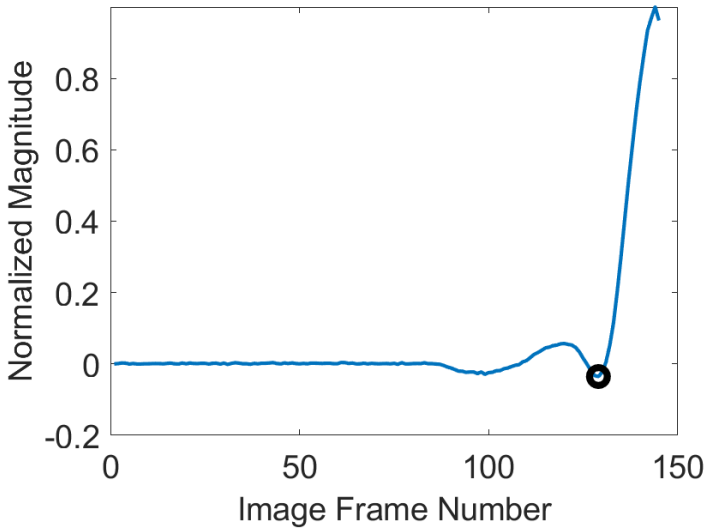

Fig. 9 Normalized magnitude of the average color value in the blue-orange channel for the sample throughout the course of the experiment. The local minimum prior to the spike represents the beginning of mechanochromism.

4.2 Results

Figure 10 shows a typical experiment for a sample embedded with the **t-SP** molecule. After impact, the SP-embedded PDMS remains blue for several minutes. A comparison between the **b-SP** and **t-SP** samples (Table 2) shows the number of covalent attachments between SP and the bulk PDMS exerts little influence on both onset stress and strain. Both onset stress and onset strain are similar within the margin of error (one standard deviation = ±4% strain). The data for the two studied SPs are shown in Fig. 11.

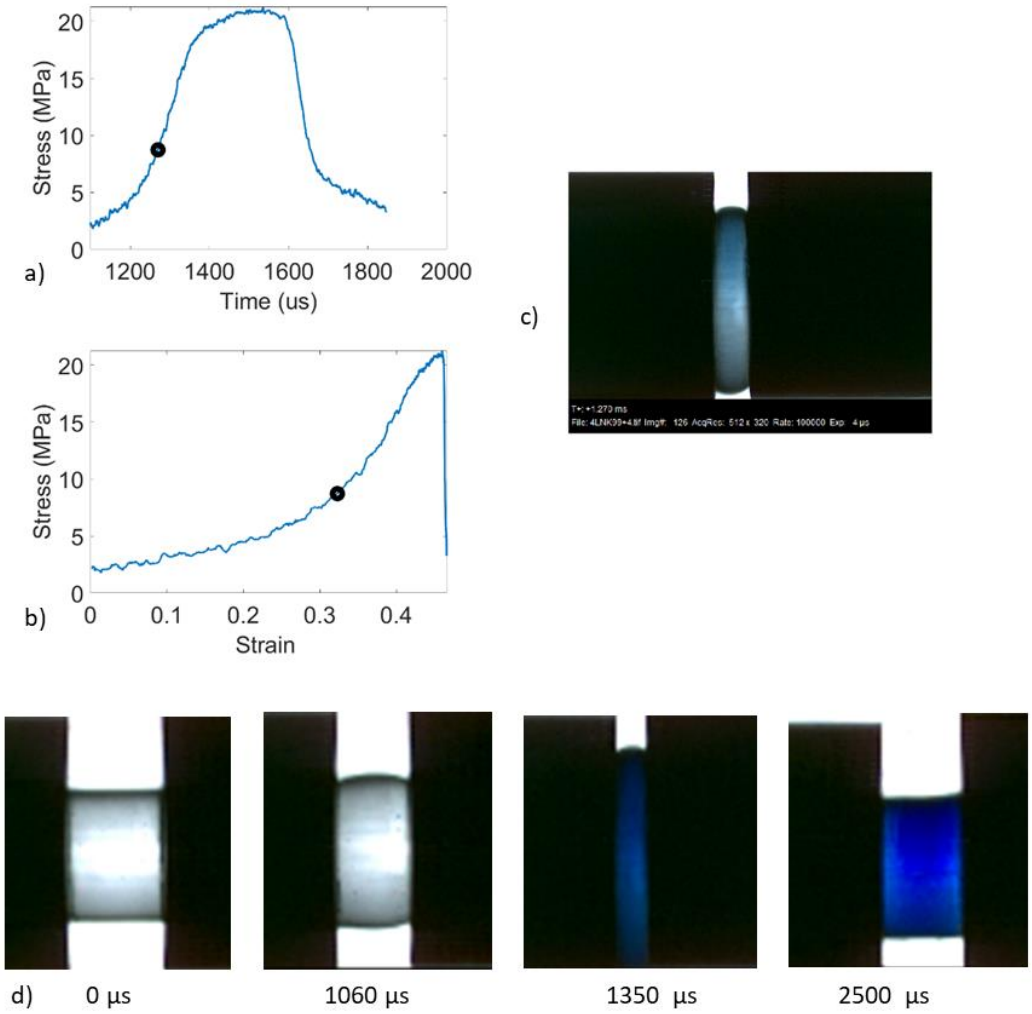

Fig. 10 Stress–time (a) and stress–strain curves (b) are shown for a typical experiment. (c) The sample at the onset of mechanochromic response. (d) A series of images showing the sample at different times during the course of the experiment.

Table 2 The average peak stress and peak strain as well as the average onset stress and onset strain at the onset of mechanochromism is shown for both b-SP (9) and t-SP (1) embedded PDMS samples. The margin of error represents one standard deviation.

Sample	Peak stress (MPa)	Peak strain	Onset stress (MPa)	Onset strain
b-SP (9)	19.9 ± 1.66	0.52 ± 0.05	6.1 ± 0.89	0.34 ± 0.03
t-SP (1)	19.3 ± 1.64	0.51 ± 0.05	7.4 ± 1.00	0.37 ± 0.04

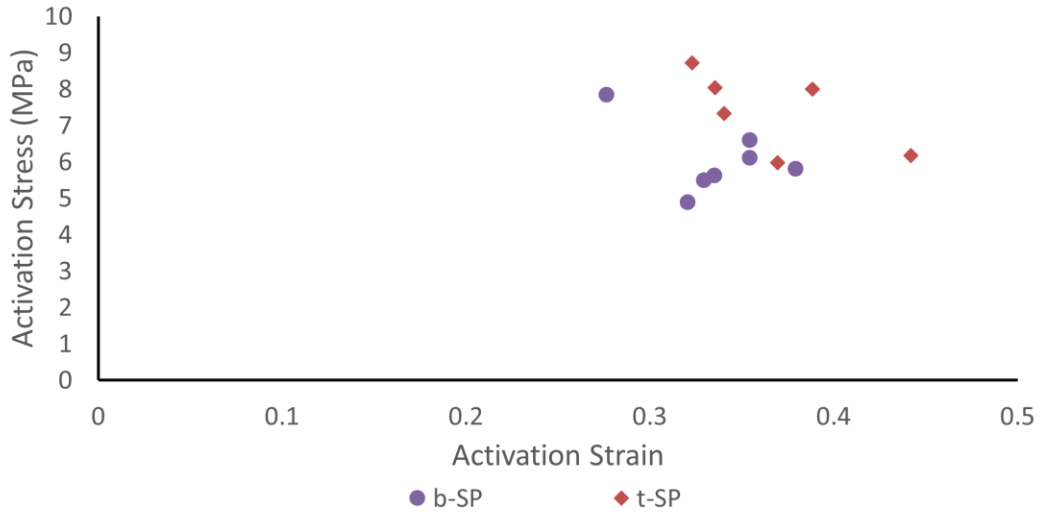

Fig. 11 Stress and strain at the onset of mechanochromism is shown for each sample for the b-SP and t-SP embedded PDMS

5. Discussion

The relative activation in **t-SP_A** and **t-SP_B** are aligned with expectations, as reducing mechanophore concentration by 50% results in a proportional reduction in the colorimetric response of the elastomer. In contrast, however, a comparison of four-arm and two-arm mechanophores runs counter to our expectations. In particular, we hypothesized that the dendritic cross-linker architecture would act as a "force funnel" that would lead to increased activation in **t-SP_A** relative to **b-SP**. Instead, the opposite is observed; activation in **b-SP** is approximately 30% higher than in **t-SP_A**, even though the total concentration of mechanophore is the same and the four-arm mechanophore in **t-SP_A** is more extensively cross-linked into the network.

There are two potential origins for the differential activation. First, it is possible the minor changes in network structure that lead to different tensile mechanical behavior in **t-SP_A** and **b-SP** are responsible for the differences in molecular response. Possible contributions from network structure are suggested by time-

dependent activation/deactivation studies described below. Second, the differential response might be primarily due to the molecular architecture within an otherwise effectively identical network. For example, simulations of highly strained networks reveal the presence of highly stressed "force chains"[27] that span the simulation box, while strands outside of the force chains experience relatively low tension. It is possible the tetra-arm architecture provides a mechanism for macroscopic stress to effectively "short circuit" the intended force-funneling pathway; for example, by two alkenes on the same side of the mechanophore joining the primary force chain to the exclusion of the mechanophore. In **t-SP**, the end-to-end distance between alkene functionalities that cross the SP mechanophore is longer than that between alkenes on the same side of the mechanophore, and force tends to focus on the shorter cross-linkers within a strained network. Further studies will be needed to better understand these empirical observations.

From the high-rate data, it appears both the average onset strain and stress for SP molecules **1** and **9** are within experimental error of each other, showing little to no effect from the additional connections to the PDMS backbone (Table 2 and Fig. 11). This result is again interesting, as one would expect to see a stress-funneling effect for the four-arm SP **1**, where the force applied is more efficiently transferred to the SP core due to the greater number of connections to the polymeric backbone. However, recent work from our group showing high-rate experiments conducted on two-arm SP mechanophores[15,16] describes that although stress inhomogeneities may be present due to the high-force fractions experienced in a select area of the sample, they are overtaken by chain tension-related dynamics. In the present case, this may explain the similar activation in the four-arm SP **1** compared to the two-arm SP **9**. Despite greater molecular differences (even those that involve more connections to the polymer backbone), chain dynamics determine onset activation.

As mentioned previously, Otsuka and coworkers observed more activation in branched PS polymers relative to linear polymers.[19,20] They attributed the enhanced activation to the improved entanglement and inhibited mobility, pertaining to recombination of generated radical species resulting from branched polymer architectures. Due to the high T_g (~105 °C) and therefore poor chain mobility of the PS polymer, transduction of force to the mechanophore due to compression or stretch contributions is minimal, and the PS polymer typically experiences failure prior to the point at which mechanophore activation would occur. With this said, PS is a more-rigid polymeric system as compared to PDMS. The authors of the PS study note that with their dendrimer-type molecules, force is more readily transferred to the dendrimer/mechanophore core due to the more-rigid structure that arises from a high surface density.[20] This rigidity prevents force attenuation, and

therefore more effectively transfers force to the core of the dendrimer, where the mechanophore is located. In our present work, the elastomeric PDMS chains have greater mobility (a low T_g of –125 °C) in the presence of a constrained force, and can more effectively attenuate that force through chain movement and slippage, thereby preventing the mechanophore from experiencing the full applied mechanical force. For the PS study, grinding was the source of force in their experiments and the exact nature of the strain and mechanisms of stress transfer are therefore complex. The PDMS elastomers used here employ strain/stretching for generation of tension within the polymer chain. As a result of the differences in both T_g and mechanical loading, the means by which mechanical force is transferred to the SP mechanophore in the strained PDMS network is fundamentally different from the PS work,[19,20] thus complicating a direct comparison between the two systems.

Finally, possible time-dependent contributions to the relative activation between four-arm and two-arm mechanophores were considered. When held at a constant strain of 130%, the mechanochromism evolves differently in **b-SP** and **t-SP_A**. As seen in Fig. 12, the mechanochromism of **b-SP** increases and plateaus at 10 min, whereas the absorption of **t-SP_A** slowly decreases over the same time. This reduction is a result of relaxation of activated SP and may be due to the absence of tension applied across the SP mechanophore. In other words, the SP cross-linker in **t-SP_A** was stretched to a threshold force, followed by a decrease in tension after the activation event. The absence of constant tension along the SP cross-linker could be attributed to the Mullins' effect,[28,29] that is, hysteresis in the stress–strain behavior of filled rubbers due to scission of physical/chemical bonding between polymer chains and the silica filler particles (~10-nm particle size), which is known to impact mechanophore response in Sylgard 184.[30] Regardless, under the relatively slow loading conditions of the quasi-static experiment, the loss of color in **t-SP_A** might account for some of the differences in response relative to **b-SP**, and explain why comparably small differences are observed in the high-rate loading experiments where less time for strand relaxation is available.

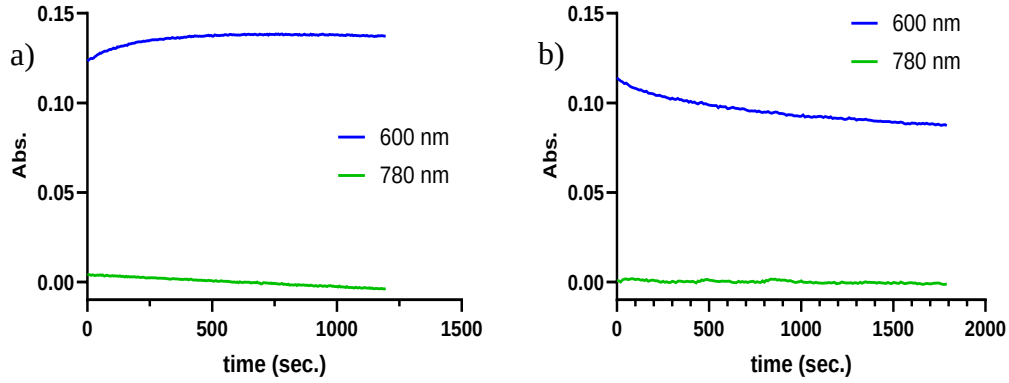

Fig. 12 b-SP (a) and t-SP_A (b) samples were stretched and maintained at 130% strain, and the absorbance at 600 nm (peak absorption of MC) and 780 nm (used as reference absorption here) was monitored over time

6 Additional Modifications to Curing

6.1 Optimization of PDMS Curing without Fillers

The modified PDMS network, without filler particles, contains a mixture of long (L) and short (S) chain PMDS bases, as well as PDMS junctions (Fig. 13). The PDMS base is composed of two chain-end vinyl groups, and the PDMS junction contains, on average, 6.6 hydrosilane (Si-H) groups along the polymer backbone. The platinum-catalyzed hydrosilylation between base and junction allows for formation of the polymer network (Table 3).

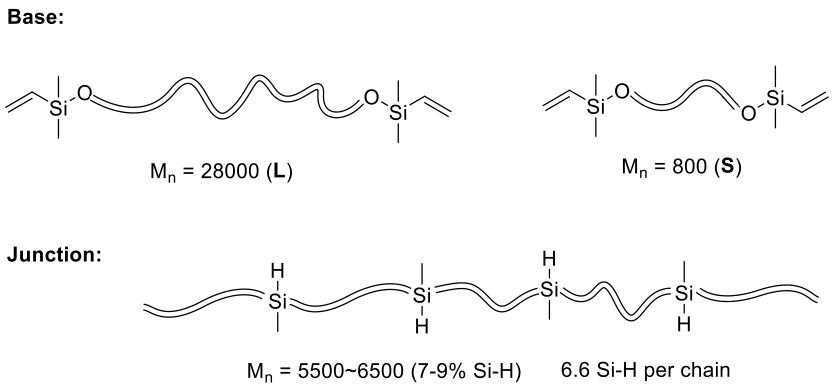

Fig. 13 The long (L) and short (S) base groups as well as the junction chains used in curing experiments without fillers

Table 3 Formulation of PDMS elastomers without fillers

	Base		Junction		[Pt] cat.
	m	n (vinyl)	m	n (Si-H)	
L	0.5 g	8.55e-6 mol	0.05 g	5.5e-5 mol	200 ppm/vinyl
S	0.5 g	3.57e-5 mol	0.05 g	5.5e-5 mol	200 ppm/vinyl

To obtain a PDMS network with desirable mechanical properties, the molar ratio of long (L) and short (S) chain bases was adjusted (Table 4).

Table 4 Formulation of PDMS elastomers without fillers. The ratio of long chains to short chains were varied.

L/S	Base			Junction		[Pt] cat.
	L	S	n (vinyl)	m	n (Si-H)	
1:9	0.5 g	0.13 g	3.57e-4 mol	0.5 g	5.5e-4 mol	200 ppm/vinyl
3:7	0.6 g	0.04 g	1.43e-4 mol	0.2 g	2.2e-4 mol	200 ppm/vinyl
5:5	0.5 g	0.14 g	7.15e-5 mol	0.1 g	1.1e-4 mol	200 ppm/vinyl

The total molar numbers of vinyl groups (n (vinyl)) and hydrosilane groups (n (Si-H)) are indicated (Tables 3 and 4), and the ratio of these two functionalities was set to n (vinyl)/n (Si-H) = 0.65. After the PDMS base and junction were vortexed for 2 min, a corresponding amount of Karstedt's catalyst solution,[31] a divinyl siloxane platinum complex, (32.8 mg in 100 mL xylene) was added. The resulting clear mixture was vortexed and cured at 65 °C overnight.

6.2 Results and Discussion

To determine if the Mullins effect was influencing activation of the four-arm SP **1**, several SP-embedded PDMS networks, were prepared, without filler, using combinations of L/S chain bases and junction mixtures (Tables 3 and 4). The formulation using only L base did not cure after overnight heating, whereas the formulation using only S base gave a clear and soft film (Fig. 14a and b). Manual stretching of the S-based film to break gave no mechanoactivation of the **t-SP 1**-embedded sample, and the clear-blue mechanochromism was only observed after multiple rounds of compression of the sample (Fig. 14c and d).

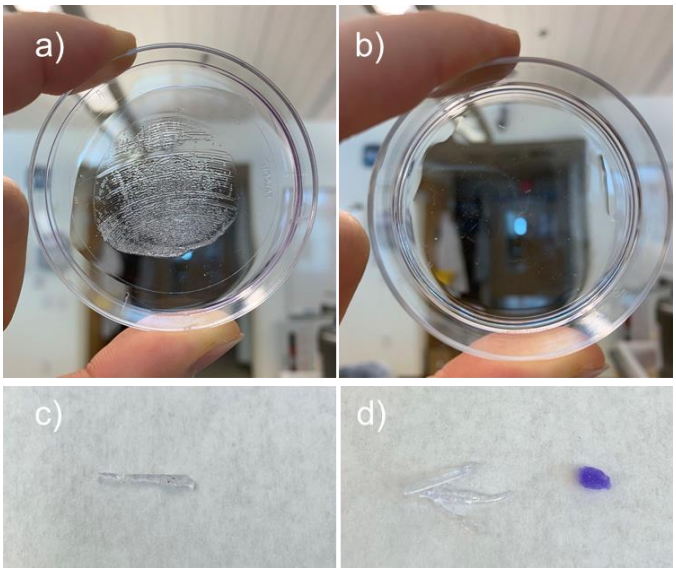

Fig. 14 t-SP 1-embedded PDMS network prepared from L (a) and S (b) bases. Pure L base resulted in an uncured mixture while pure S base gave a clear, soft film. Stretching (c) and squeezing (d) of the cured film prepared from pure S base.

The PDMS network, without filler, was optimized using a long/short (L/S) mixing strategy,[32] which had proven effective for preparing PDMS polymer networks with enhanced mechanical properties (Table 4). The curing ratio of L:S = 3:7 provided the best mechanical properties among the mixed PDMS networks without added **t-SP 1** mechanophore (Fig. 15). However, attempted incorporation of **t-SP 1** or **b-SP 9** mechanophores resulted in a mixture that was unable to be cured into a PDMS film. This result demonstrates the filler is necessary for the proper incorporation of these mechanophores into cured Sylgard 184 PDMS. Unfortunately, the same filler that enables incorporation of these mechanophores may also affect their mechanochemical properties, possibly by influencing stress concentration areas at the filler particle/mechanophore interface.[33,34]

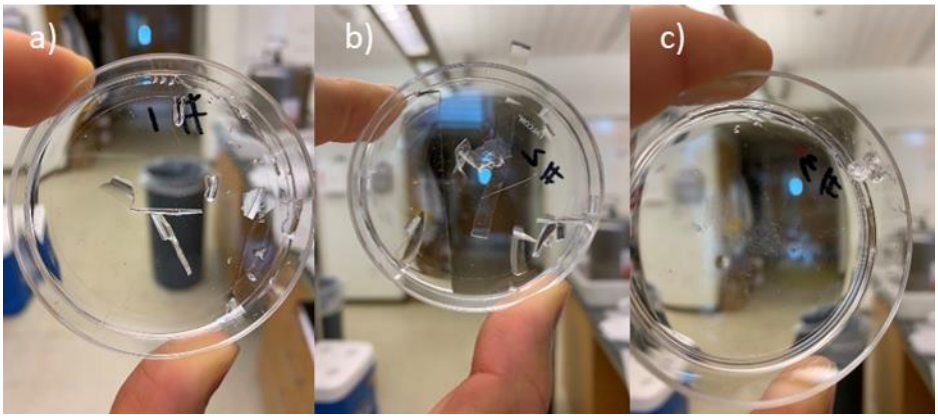

Fig. 15 PDMS network, without fillers, prepared with various L/S ratios. (a) L/S = 1:9 produced a brittle film; (b) L/S = 3:7 gave film with some elasticity; (c) L/S = 5:5 afforded a soft and sticky film.

7. Conclusion

In conclusion, it has been found that a SP mechanophore **1** with four branch arms connected to the backbone of an elastomeric system (PDMS) does not provide increased activation, as compared to a traditional two-arm SP, under both quasi-static and high-rate loading. This finding was unexpected, as it was hypothesized that the additional branch arms would funnel force to the SP mechanophore and allow easier activation, as has been shown in a PS system. The nature of the elastomeric structure, where significant chain mobility as well as chain slippage enables force attenuation, likely plays a considerable role in the observed activity. Previous studies on dendritic structures used grinding as the activation method, which causes shear stress that may be more significant for activation in a rigid system, such as PS. This is in contrast to the tension used to activate the SP mechanophores in the elastomeric system studied here. Lastly, the polymer/filler particle interface appears to be important for determining both mechanophore and curing activity, as omission of the filler particles prevents the PDMS from being cured to produce a specimen with mechanoresponsive properties. Studies focusing on SP mechanophores with a greater number of branch arms are ongoing to elucidate if the results found in this study extend to that of higher-order dendritic compounds.

8. References

1. Caruso MM, Davis DA, Shen Q, Odom SA, Sottos NR, White SR, Moore JS. Mechanically-induced chemical changes in polymeric materials. Chem Rev. 2009;109(11):5755–5798.
2. Li J, Nagamani C, Moore JS. Polymer mechanochemistry: from destructive to productive. Acc Chem Res. 2015;48(8):2181–2190.
3. Klajn R. Spiropyran-based dynamic materials. Chem Soc Rev. 2014;43(1):148–184.
4. Li M, Zhang Q, Zhou Y-N, Zhu S. Let spiropyran help polymers feel force! Prog Polym Sci. 2018;79:26–39.
5. Robb MJ, Kim TA, Halmes AJ, White SR, Sottos NR, Moore JS. Regioisomer-specific mechanochromism of naphthopyran in polymeric materials. J Am Chem Soc. 2016;138(38):12328–12331.
6. Ramirez ALB, Kean ZS, Orlicki JA, Champhekar M, Elsakr SM, Krause WE, Craig SL. Mechanochemical strengthening of a synthetic polymer in response to typically destructive shear forces. Nature Chem. 2013;5:757–761.
7. Kean ZS, Gossweiler GR, Kouznetsova TB, Hewage GB, Craig SL. A coumarin dimer probe of mechanochemical scission efficiency in the sonochemical activation of chain-centered mechanophore polymers. Chem Comm. 2015;51(44):9157–9160.
8. Potisek SL, Davis DA, Sottos NR, White SR, Moore JS. Mechanophore-linked addition polymers. J Am Chem Soc. 2007;129(45):13808–13809.
9. Stratigaki M, Göstl R. Methods for exerting and sensing force in polymer materials using mechanophores. ChemPlusChem. 2020;85(6):1095–1103.
10. Davis DA, Hamilton A, Yang J, Cremar LD, Van Gough D, Potisek SL, Ong MT, Braun PV, Martinez TJ, White SR, Moore JS, Sottos NR. Force-induced activation of covalent bonds in mechanoresponsive polymeric materials. Nature. 2009;459:68–72.
11. Beiermann BA, Kramer SLB, May PA, Moore JS, White SR, Sottos NR. The effect of polymer chain alignment and relaxation on force-induced chemical reactions in an elastomer. Adv Funct Mater. 2014;24(11):1529–1537.
12. Kingsbury CM, May PA, Davis DA, White SR, Moore JS, Sottos NR. Shear activation of mechanophore-crosslinked polymers. J Mater Chem. 2011;21(23):8381–8388.

13. Hemmer JR, Smith PD, van Horn M, Alnemrat S, Mason BP, de Alaniz JR, Osswald S, Hooper JP. High strain-rate response of spiropyran mechanophores in PMMA. J Polym Sci Polym Phys. 2014;52(20):1347–1356.

14. Gossweiler GR, Hewage GB, Soriano G, Wang Q, Welshofer GW, Zhao X, Craig SL. Mechanochemical activation of covalent bonds in polymers with full and repeatable macroscopic shape recovery. ACS Macro Lett. 2014;3(3):216–219.

15. Shannahan L, Berry J, Lin Y, Barbee M, Craig S, Casem D, Fermen-Coker M. A mechanochemistry-based technique for early material damage detection in high strain rate processes. Aberdeen Proving Ground (MD): Army Research Laboratory (US); 2019 Jan. Report No.: ARL-TR-8629.

16. Shannahan LS, Lin Y, Berry JF, Barbee MH, Fermen-Coker M, Craig SL. Onset of mechanochromic response in the high strain rate, uniaxial compression of spiropyran embedded silicone elastomers. Macro Rapid Comm. Forthcoming.

17. Lee CK, Beiermann BA, Silberstein MN, Wang J, Moore JS, Sottos NR, Braun PV. Exploiting force sensitive spiropyrans as molecular level probes. Macromolecules. 2013;46(10):3746–3752.

18. Vidavsky Y, Yang SJ, Abel BA, Agami I, Diesendruck CE, Coates GW, Silberstein MN. Enabling room-temperature mechanochromic activation in a glassy polymer: synthesis and characterization of spiropyran polycarbonate. J Am Chem. Soc. 2019;141(25):10060–10067.

19. Oka H, Imato K, Sato T, Ohishi T, Goseki R, Otsuka H. Enhancing mechanochemical activation in the bulk state by designing polymer architectures. ACS Marco Lett. 2016;5(10):1124–1127.

20. Watabe T, Ishizuki K, Aoki D, Otsuka H. Mechanochromic dendrimers: the relationship between primary structure and mechanochromic properties in the bulk. Chem Comm. 2019;55(48):6831–6834.

21. Berry JF. Facile isolation of functionalized spiropyran mechanophores without recrystallization. Aberdeen Proving Ground (MD): Army Research Laboratory (US); 2018 Sept. Report No.: ARL-CR-0830.

22. Carlmark A, Malmström E, Malkoch M. Dendritic architectures based on bis-MPA: functional polymeric scaffolds for application driven research. Chem Soc Rev. 2013;42(13):5858–5879.

23. Montañez MI, Campos LM, Antoni P, Hed Y, Walter MV, Krull BT, Khan A, Hult A, Hawker CJ, Malkoch M. Accelerated growth of dendrimers via thiol-ene and esterification reactions. Macromolecules. 2010;43(14):6004–6013.

24. Lin Y, Barbee MH, Chang C-C, Craig SL. Regiochemical effects on mechanophore activation in bulk materials. J Am Chem Soc. 2018;140(46):15969–15975.

25. Chen WW, Song B. Split Hopkinson (Kolsky) bar: design, testing and applications. Berlin (Germany): Springer Science & Business Media; 2010.

26. Bacon C. An experimental method for considering dispersion and attenuation in a viscoelastic Hopkinson bar. Exp Mech. 1998;38(4):242–249.

27. Adhikari R, Makarov DE. Mechanochemical kinetics in elastomeric polymer networks: heterogeneity of local forces results in nonexponential kinetics. J Phys Chem B. 2017;121(10):2359–2365.

28. Mullins L. Softening of rubber by deformation. Rub Chem Tech. 1969;42(1):339–362.

29 Diani J, Fayolle B, Gilormini P. A review on the Mullins effect. Eur Poly J. 2009;45(3):601–612.

30. Clough JM, Creton C, Craig SL, Sijbesma RP. Covalent bond scission in the Mullins effect of a filled elastomer: real-time visualization with mechanoluminescense. Adv Funct Mater. 2016;26(48):9063–9074.

31. Karstedt BD, inventor; General Electric Co, assignee. Platinum complexes of unsaturated siloxanes and platinum containing organopolysiloxanes. United States patent 3775452. 1973 Nov 27.

32. Llorente MA, Andrady AL, Mark JE. Model networks of end-linked polydimethylsiloxane chains. Coll Polym Sci. 1981;259:1056–1061.

33. Zhang Y, Lund E, Gossweiler GR, Lee B, Niu Z, Khripin C, Munch E, Couty M, Craig SL. Molecular damage detection in an elastomer nanocomposite with a coumarin dimer mechanophore. Macromol Rapid Comm. 2020;2000359 (Early View).

34. Grady ME, Birrenkott CM, May PA, White SR, Moore JS, Sottos NR. Localization of spiropyran activation. Langmuir. 2020;36(21):5847–5854.

Appendix. Synthetic Methods

Most solvents were purchased from either Sigma-Aldrich or VWR International and used as is, except absolute ethanol, which was purchased from Koptec, Inc. $CDCl_3$ was purchased from Sigma-Aldrich, and DMSO-d_6 was purchased from Cambridge Isotope Laboratories. All other reagents were purchased from either Sigma-Aldrich or Alfa Aesar. All glassware was dried in an oven set to 110 °C, and reactions were stirred magnetically under an argon atmosphere. Thin-layer chromatography (TLC) was performed using EMD/Millipore Silica Gel 60 TLC plates (250 µm, F_{254} indicator) and viewed under UV light (254 nm). Column chromatography was performed using SiliCycle SiliaFlash F60 silica gel (40–63-µm particle size, 230–400 mesh). ^{1}H-NMR and ^{13}C-NMR were performed on a Bruker 400-MHz nuclear magnetic resonance (NMR) system. NMR values are reported in parts per million (ppm) as compared to the reference peaks of $CDCl_3$ (7.26 ppm for ^{1}H and 77.16 ppm for ^{13}C) and DMSO-d_6 (2.50 ppm for ^{1}H and 39.52 ppm for ^{13}C). ^{1}H-NMR values are reported as (chemical shift in ppm, multiplicity, coupling constant in hertz, relative integral). ^{1}H-NMR multiplicities are indicated as s (singlet), d (doublet), t (triplet), dd (doublet of doublets), td (triplet of doublets), m (multiplet), and b (broad). DCM is dichloromethane, THF is tetrahydrofuran, MeOH is methanol, NaOH is sodium hydroxide, HCl is hydrochloric acid, $NaHCO_3$ is sodium bicarbonate, Na_2SO_4 is sodium sulfate.

3-(allyloxy)-2-((allyloxy)methyl)-2-methylpropanoic acid (7)

Prepared according to a slightly modified literature procedure.[1] 3-hydroxy-2-(hydroxymethyl)-2-methylpropanoic acid (bis-MPA) **2** (5.00 g, 37.3 mmol, 1 equiv.) and NaOH (14.92 g, 0.37 mol, 10 equiv.) were stirred in 75 mL toluene at room temperature. This suspension was heated to 110 °C and allyl bromide (22.6 mL, 0.26 mol, 7 equiv.) was added and the solution refluxed overnight with vigorous stirring. The resulting suspension was cooled to room temperature and the organic layer removed through rotary evaporation. To dissolve the solid residue, 125 mL of water was added and concentrated HCl was added slowly until the pH was approximately 1. The aqueous solution was then extracted two times with dichloromethane (100 mL × 2), the organic layers combined, dried with Na_2SO_4 and the solvent removed via rotary evaporation to give 3-(allyloxy)-2-((allyloxy)methyl)-2-methylpropanoic acid **7** as a light-yellow oil (6.47 g, 81% yield) that was used without further purification. ^{1}H-NMR (400 MHz, $CDCl_3$) δ 10.70 (bs, 1H), 5.86 (m, 2H), 5.25 (d, J = 17.2 Hz, 2H), 5.15 (d, J = 10.4 Hz, 2H), 3.99 (d, J = 5.5 Hz, 4H), 3.55 (d, J = 4.2 Hz, 4H), 1.23 (s, 3H). ^{13}C-NMR (100 MHz, $CDCl_3$) δ 180.4, 134.6, 116.9, 72.4, 71.9, 48.2, 17.9.

[1] Montañez MI, Campos LM, Antoni P, Hed Y, Walter MV, Krull BT, Khan A, Hult A, Hawker CJ, Malkoch M. Accelerated growth of dendrimers via thiol-ene and esterification reactions. Macromolecules. 2010;43(14):6004–6013.

3-(allyloxy)-2-((allyloxy)methyl)-2-methylpropanoic anhydride (8)

Prepared according to a slightly modified literature procedure.[1] 3-(allyloxy)-2-((allyloxy)methyl)-2-methylpropanoic acid **7** (2.50 g, 11.7 mmol, 1.0 equiv.) was dissolved in 6 mL dry DCM and stirred 5 min under an argon atmosphere. Dicyclohexylcarbodiimide (DCC) (1.21 g, 5.85 mmol, 0.5 equiv.), dissolved in 3-mL dry DCM, was added dropwise over 5 min at room temperature. The reaction turned cloudy and was stirred for 48 h under argon. The suspension was filtered and the solvent removed via rotary evaporation to give a cloudy suspension. This material was then dissolved in 40 mL hexane and cooled in an ice bath for 10 min. The remaining solution was filtered through a 0.2-µm filter and the solvent removed under rotary evaporation to give 3-(allyloxy)-2-((allyloxy)methyl)-2-methylpropanoic anhydride **8** (3.93 g, 82% yield) as a light-yellow oil that was used without further purification. ^{1}H-NMR (400 MHz, $CDCl_3$) δ 5.91-5.81 (m, 4H), 5.25 (d, *J* = 17.2 Hz, 4H), 5.15 (d, *J* = 10.4 Hz, 4H), 3.98 (d, *J* = 5.4 Hz, 8H), 3.57 (s, 8H), 1.26 (s, 6H). ^{13}C-NMR (100 MHz, $CDCl_3$) δ 169.6, 134.6, 116.8, 72.4, 71.5, 49.9, 17.3.

2-(8-((3-(allyloxy)-2-((allyloxy)methyl)-2-methylpropanoyl)oxy)-3',3'-dimethyl-6-nitrospiro[chromene-2,2'-indolin]-1'-yl)ethyl 3-(allyloxy)-2-((allyloxy)methyl)-2-methylpropanoate (1)

To a mixture of 1'-(2-hydroxyethyl)-3',3'-dimethyl-6-nitrospiro[chromene-2,2'-indolin]-8-ol **5**[2] (0.25 g, 0.68 mmol, 1 equiv.) in 8 mL dry tetrahydrofuran (THF) was added *N*,*N*-dimethylaminopyridine (DMAP) (0.062 g, 0.51 mmol, 0.75 equiv.) and the mixture stirred for 5 min under argon. Then, 3-(allyloxy)-2-((allyloxy)methyl)-2-methylpropanoic anhydride **8** (0.61 g, 1.49 mmol, 2.2 equiv.), in 3-mL dry THF, was added dropwise over 3.5 h via syringe pump. Reaction was stirred for 96 h at room temperature and the solvent was removed under rotary evaporation. The residue was dissolved in 60-mL DCM and washed twice with 100-mL saturated $NaHCO_3$, once with 75-mL 1M HCl, once with 50-mL water, and once with 50-mL brine. The organic layer was dried over Na_2SO_4 and the solvent removed under rotary evaporation. The residue was purified via column chromatography, using a gradient of DCM to 0.5% MeOH in DCM to give 2-(8-((3-(allyloxy)-2-((allyloxy)methyl)-2-methylpropanoyl)oxy)-3',3'-dimethyl-6-nitrospiro[chromene-2,2'-indolin]-1'-yl)ethyl 3-(allyloxy)-2-((allyloxy)methyl)-2-methylpropanoate **1** (0.19 g, 36% yield) as a purple oil. ^{1}H-NMR (400 MHz, $CDCl_3$) δ 7.93 (d, *J* = 2.6 Hz, 1H), 7.79 (d, *J* = 2.6 Hz, 1H), 7.13 (td, *J* = 7.8,1.2

[2] Berry JF. Facile isolation of functionalized spiropyran mechanophores without recrystallization. Aberdeen Proving Ground (MD): Army Research Laboratory (US); 2018 Sept. Report No.: ARL-CR-0830.

Hz, 1H), 7.04 (dd, *J* = 7.4,1.0 Hz, 1H), 6.95 (d, *J* = 10.4 Hz, 1H), 6.84 (t, *J* = 7.2 Hz, 1H), 6.65 (d, *J* = 7.8 Hz, 1H), 5.99 (d, *J* = 10.5 Hz, 1H), 5.91-5.76 (m, 4H), 5.26 (m, 1H), 5.23-5.16 (m, 4H), 5.16-5.08 (m, 3H), 4.26-4.15 (m, 2H), 3.93-3.80 (m, 8H), 3.53-3.47 (m, 6H), 3.33 (t, *J* = 5.6 Hz, 2H), 3.26 (m, 2H), 1.25 (s, 3H), 1.17 (s, 3H), 0.65 (s, 3H). ^{13}C-NMR (100 MHz, $CDCl_3$) δ 174.8, 171.6, 151.1, 146.8, 140.4, 137.5, 135.9, 135.0, 134.9, 134.9, 128.4, 127.9, 121.8, 121.7, 120.3, 120.2, 119.6, 119.4, 116.7, 116.7, 116.7, 116.6, 107.4, 107.3, 72.4, 72.4, 72.3, 72.2, 71.3, 71.2, 62.9, 52.3, 48.6, 48.5, 42.5, 26.2, 195, 18.1, 17.1.

List of Symbols, Abbreviations, and Acronyms

ABF	arylbenzofuranone
ARL	Army Research Laboratory
bis-MPA	2,2-bis(hydroxymethyl)propionic acid
B/R	blue/red
CCDC	US Army Combat Capabilities Development Command
DABBF	diarylbibenzofuranone
DCC	dicyclohexylcarbodiimide
DCM	dichloromethane
DMAP	*N*,*N*-dimethylaminopyridine
g-DBCs	*gem*-dibromocyclopropanes
HCl	hydrochloric acid
L	long
MC	merocyanine
MeOH	methanol
NaOH	sodium hydroxide
NMR	nuclear magnetic resonance
PC	polycarbonate
PDMS	polydimethylsiloxane
PMA	poly(methacrylate)
PMMA	poly(methyl methacrylate)
ppm	parts per million
PS	polystyrene
PU	polyurethane
S	short
SiH	hydrosilane

SP	spiropyran
THF	tetrahydrofuran
TLC	thin-layer chromatography
UV	ultraviolet

1 (PDF) DEFENSE TECHNICAL INFORMATION CTR
DTIC OCA

1 (PDF) CCDC ARL
FCDD RLD DCI
TECH LIB

1 (PDF) APPL PHYSICS LABORATORY
Z XIA

4 (PDF) NATICK SOLDIER RES DEV ENG CTR
S FILOCAMO
C DOONA
T TIANO
B FASEL

1 (PDF) DUKE UNIVERSITY
S CRAIG

1 (PDF) STANFORD UNIVERSITY
Y LIN

2 (PDF) UNIV ILLINOIS URBANA CHAMPAIGN
J MOORE
N SOTTOS

1 (PDF) UNIVERSITY OF WISCONSIN
AJ BOYSTON

1 (PDF) UCSD
N BOECHLER

24 (PDF) CCDC ARL
FCDD RLD
P BAKER
FCDD RLR EM
D POREE
FCDD RLW
J ZABINSKI
S KARNA
A RAWLETT
S SCHOENFELD
J CIEZAK-JENKINS
FCDD RLW B
C HOPPEL
FCDD RLW M
E CHIN
FCDD RLW MA
R LAMBETH
E WETZEL
T PLAISTED
FCDD RLW MG
J LENHART
J ORLICKI
FCDD RLW P
R FRANCART
FCDD RLW PC
J BERRY
M FERMEN-COKER
L SHANNAHAN
D CASEM
J CAZAMIAS
J CLAYTON
C WILLIAMS
S TURNAGE
FCDD VTM
A HALL